Suppression of sidebands in magicanglespinning nuclear magnetic resonance: General principles and analytical solutions

Oleg N. Antzutkin, Zhiyang Song, Xiaolong Feng, and Malcolm H. Levitt

Citation: The Journal of Chemical Physics **100**, 130 (1994); doi: 10.1063/1.466983
View online: http://dx.doi.org/10.1063/1.466983
View Table of Contents: http://scitation.aip.org/content/aip/journal/jcp/100/1?ver=pdfcov
Published by the AIP Publishing

Suppression of sidebands in magic-angle-spinning nuclear magnetic resonance: General principles and analytical solutions

Oleg N. Antzutkin, Zhiyang Song, Xiaolong Feng, and Malcolm H. Levitt
Division of Physical Chemistry, Arrhenius Laboratory, University of Stockholm, S-106 91 Stockholm, Sweden

(Received 1 June 1993; accepted 22 September 1993)

Several theoretical and experimental aspects of sideband suppression in the nuclear magnetic resonance (NMR) spectra of rotating solids are considered. The principles of sideband suppression are explored using general symmetry arguments and previous treatments are examined critically. Analytical solutions are given for sideband suppression pulse sequences employing four, five, six, and nine π pulses. The analytical solutions for four π pulses are complete. Experimental demonstrations are given.

I. INTRODUCTION

High resolution solid-state nuclear magnetic resonance (NMR) spectra of spins $I=1/2$ are produced by rapid sample rotation at the magic angle $\tan^{-1}\sqrt{2}$ with respect to the static field.[1] If the spinning speed ω_r is comparable to the spread in Larmor frequencies caused by chemical shift anisotropy (CSA), the spectra contain sets of sidebands spaced in frequency by ω_r and centered at the isotropic shift frequency ω^{iso}. Although the spinning sidebands contain useful information as to the shift anisotropies, they also crowd the spectra and complicate the assignments of the isotropic shifts. Much interest was therefore generated when Dixon demonstrated a method called total suppression of spinning sidebands (TOSS).[2,3] This uses a sequence of four π pulses to prepare the magnetization components of a powder sample such that the sidebands disappear and only the centerbands (situated at the isotropic shift frequencies) are left. Under some conditions, the center band intensities can even be enhanced compared to an unmanipulated magic-angle-spinning experiment.[4–6]

Dixon originally explained his method by the removal of rotational echoes in the free induction decay. Later analyses[4–6] employed a different interpretation based on the numerical calculation of magnetization vector trajectories. Sideband suppression was explained by the "alignment of the magnetization vectors." We contrast these two interpretations below and find the "alignment" theory to be somewhat flawed.

Further methodological development of TOSS has also taken place. New sequences have been found which are shorter or employ more evenly spaced pulses. Dixon's original sequences are quite long, occupying over two full rotational periods, with two of the π pulses very close in time. The long duration of the sequences causes loss of signal for samples with a short spin–spin relaxation time T_2, and the proximity of the pulses causes timing difficulties at high spinning speeds—in extreme cases, the pulses collide and the sequence cannot be implemented at all. To avoid these problems, sequences of only two π pulses have been used which provide only partial sideband suppression.[7] Sequences of four and six π pulses have been designed which are shorter than the original TOSS sequences and more evenly spaced.[5,6,8] Nielsen *et al.*[8] designed a set of sequences with rather evenly spaced pulses, suitable for implementation at very high spinning frequencies. These sequences were found by numerical searches for solutions to the simultaneous system of four nonlinear equations (the TOSS equations) described below. There was therefore no guarantee that all solutions had been found.

Recently, we gave an analytical derivation of a symmetrical sequence of five π pulses which lasts only one single rotational period.[9] Here we present a complete set of analytical solutions for TOSS sequences involving four π pulses. This includes some new sequences which may be of interest, in particular, one sequence of rather evenly spaced π pulses and another lasting only 0.4670 of a rotational period. The latter sequence leads to frequency-dependent phase shifts of the powder-average center bands, but we show experimentally that these phase shifts can be corrected after Fourier transformation without causing unacceptable distortions. We also explore the relationship between the four pulse sequences and the new five pulse sequences.[9] We demonstrate the shortest known TOSS sequence which does not generate phase shifts, of the powder average signal consisting of five π pulses and lasting only 0.7227 of a single rotational period. All methods may be incorporated in two-dimensional pulse schemes, gaining the advantages of sideband suppression without loss of intensity or of the anisotropy information.[10–12] They also can be applied to partially ordered samples in rotor-synchronized two-dimensional experiments to reveal both the degree of molecular order and intramolecular dynamics.[13]

These new sequences provide effective competition to the recently described SELTICS sequences,[14] which use continuous radiofrequency bursts to suspend the chemical shift evolution instead of π pulses.

II. THEORY

A. General principles of sideband suppression

It was recently shown that the uniform phase of spinning sidebands in a normal powder magic-angle-spinning

 0021-9606/94/100(1)/130/11/$6.00

(MAS) experiment could be understood by general symmetry arguments.[15] Similar reasoning can be applied to the problem of sideband suppression.

Consider a disordered sample containing a number of chemically equivalent isolated spin 1/2 sites. Each of the sites is assumed to have the same isotropic shift ω^{iso}, chemical shift anisotropy $\omega_0\Delta\sigma$, and asymmetry parameter η, but a different orientation in space. If the sample is contained in a mechanical rotor, the site orientation can be specified by the three Euler angles $\Omega_{PR}=\{\alpha_{PR},\beta_{PR},\gamma_{PR}\}$ defining the relationship of the CSA principal axis frame P with a rotor fixed frame R. As the sample rotates, the angles Ω_{PR} remain constant for each crystallite, but the relative orientation of R and a fixed laboratory reference system L change in time. The relative orientation of the rotor frame R and the lab frame L is defined by the Euler angles $\Omega_{RL}=\{\omega_r t,\beta_{RL},0\}$, where $\beta_{RL}=\tan^{-1}\sqrt{2}$ for exact magic-angle spinning.

The time and orientation dependencies of the precession frequency ω of a single site can be written using a Fourier series

$$\omega(t;\Omega_{PR})=\sum_{m=-2}^{2}\omega^{(m)}(\Omega_{PR})e^{im\omega_r t} \tag{1}$$

with the Fourier components

$$\omega^{(m)}(\Omega_{PR})=\sum_{m'}A^P_{m'}D^2_{m'-m}(\Omega_{PR})d^2_{-m0}(\beta_{RL}) +\delta_{m0}\omega^{\mathrm{iso}}. \tag{2}$$

D and d are Wigner matrices and A^P is the chemical shift anisotropy tensor in its own principal axis frame[16]

$$A^P_0=\tfrac{2}{3}\omega_0\Delta\sigma,\quad A^P_1=A^P_{-1}=0,\quad A^P_2=A^P_{-2}=-\frac{2}{3\sqrt{6}}\eta\omega_0\Delta\sigma. \tag{3}$$

The discussion is simplified if we consider only a carousel of sites which can be brought into coincidence by a rotation around the spinning axis. The members of a carousel c experience the same cycle of spin precession frequencies, but at different times. In the present context, a carousel is formed by those chemically equivalent sites with the same values of α_{PR} and β_{PR}, but different values of γ_{PR}. Indicating α_{PR} and β_{PR} by a carousel index c and writing γ_{PR} as γ, the precession frequency can be written

$$\omega_c(t;\gamma)=\sum_m\omega_c^{(m)}(\gamma)e^{im\omega_r t}, \tag{4}$$

where the complex components $\omega_c^{(m)}(\gamma)$ have the symmetry

$$\omega_c^{(m)}(\gamma)=[\omega_c^{(-m)}(\gamma)]^*,\quad \omega_c^{(m)}(\gamma)=\omega_c^{(m)}(0)e^{im\gamma}. \tag{5}$$

It is assumed that there is a continuous uniform distribution of γ around the carousel. This encompasses finely divided powders and uniaxially ordered samples with the orientation axis coinciding with the spinning axis. The same concept applies equally well to the case of a cylindrical liquid sample rotating in an inhomogeneous magnetic field.[15] In general, there will be many such carousels, with different values of α_{PR} and β_{PR}. There may also be a number of chemically distinct sites with different isotropic shifts and shift anisotropies. These also form distinct carousels. For simplicity, we deal with the carousels one at a time.

The time-average precession frequency $\omega_c^{(0)}(\gamma)$ for any one carousel is independent of the angle γ. If the rotation angle β_{RL} is equal to the magic angle $\tan^{-1}\sqrt{2}$, this is equal to the isotropic shift frequency

$$\omega_c^{(0)}=\omega_c^{\mathrm{iso}}.$$

However, the following arguments do not depend on this property.

Suppose (-1)-quantum coherences are prepared at time $t=0$ with the same amplitude, but possibly different phases $\phi_c(0;\gamma)$. For isolated spins in high field, the rotation of the sample does not induce any transitions between different nuclear spin states, and the signal from the component γ of the carousel c at time $t\geqslant 0$ is proportional to

$$s_c(t;\gamma)=\exp\{i[\Phi_c(t,0;\gamma)+\phi_c(0;\gamma)]\} \tag{6}$$

with the integrated phase function Φ_c defined by

$$\Phi_c(t_b,t_a;\gamma)=\int_{t_a}^{t_b}dt\,\omega_c(t;\gamma). \tag{7}$$

Using Eq. (4), the integrated phase can be written

$$\Phi_c(t_b,t_a;\gamma)=\omega_c^{(0)}(t_b-t_a)+\xi_c(t_b;\gamma)-\xi_c(t_a;\gamma) \tag{8}$$

with the real function ξ_c defined by

$$\xi_c(t;\gamma)=\sum_{m\neq 0}\frac{\omega_c^{(m)}(\gamma)e^{im\omega_r t}}{im\omega_r}. \tag{9}$$

Hence, the signal component can be written

$$s_c(t;\gamma)=\exp\{i[\omega_c^{(0)}t+\xi_c(t;\gamma)-\xi_c(0;\gamma)+\phi_c(0;\gamma)]\}, \tag{10}$$

where T_2 decay is ignored for simplicity.

Now, since the function $\xi_c(t;\gamma)$ has the symmetry

$$\xi_c(t+n\tau_r;\gamma)=\xi_c(t;\gamma), \tag{11}$$

where the period $\tau_r=2\pi/\omega_r$ and n is an integer, it follows that each signal contribution has the symmetry

$$s_c(t+n\tau_r;\gamma)=s_c(t;\gamma)e^{i\omega_c^{(0)}n\tau_r} \tag{12}$$

and can be written as a Fourier series

$$s_c(t;\gamma)=\sum_{k=-\infty}^{\infty}a_c^{(k)}(\gamma)\exp[i(\omega_c^{(0)}+k\omega_r)t] \tag{13}$$

with complex coefficients $a_c^{(k)}(\gamma)$. These coefficients represent the complex amplitudes of sidebands located at frequencies $\omega_c^{(0)}+k\omega_r$. A real, positive value for $a_c^{(k)}$ indicates a positive absorption sideband; an imaginary value for $a_c^{(k)}$ indicates a dispersion mode sideband. The total signal contribution from the entire carousel is given by

$$\langle s_c(t)\rangle=(2\pi)^{-1}\int_0^{2\pi}d\gamma\,s_c(t;\gamma) \tag{14}$$

and can be written

$$\langle s_c(t)\rangle = \sum_{k=-\infty}^{\infty} \langle a_c^{(k)}\rangle \exp[i(\omega_c^{(0)}+k\omega_r)t]. \quad (15)$$

The carousel-average sideband intensities are $\langle a_c^{(k)}\rangle$.

It has been shown that if all coherences are prepared with the same phase at time 0 [$\phi_c(0;\gamma)=0$, independent of γ], then the γ-averaged sideband intensities $\langle a_c^{(k)}\rangle$ are real and positive.[15] All sidebands are in positive absorption for a normal magic-angle-spinning spectrum of a powder.

In TOSS, the situation is different. A special pulse sequence is used to prepare different initial phases for the carousel members. All pulse sequences used to date prepare the magnetization components with initial phases satisfying

$$\phi_c(0;\gamma)=\xi_c(0;\gamma)+\omega_c^{(0)}\tau_{\rm seq}, \quad (16)$$

where $\tau_{\rm seq}$ is a constant, dependent on the pulse sequence used for preparation. It is shown later how this condition is achieved for some specific pulse sequences.

Let us examine the consequences of the assumption Eq. (16). The TOSS signals can be written in the form

$$s_c^{\rm TOSS}(t;\gamma)=\exp\{i[\omega_c^{(0)}(t+\tau_{\rm seq})]\}f_c(\omega_r t+\gamma), \quad (17)$$

where the function f_c is defined[13]

$$f_c(\psi)=\exp\left[\sum_{m\neq 0}\frac{\omega_c^{(m)}(0)e^{im\psi}}{m\omega_r}\right]. \quad (18)$$

The center band amplitude in the TOSS experiment is given by the Fourier component of $s_c^{\rm TOSS}(t;\gamma)$ at frequency $\omega_c^{(0)}$,

$$a_c^{(0)}(\gamma)^{\rm TOSS}=\tau_r^{-1}\int_0^{\tau_r} dt\, s_c^{\rm TOSS}(t;\gamma)\exp(-i\omega_c^{(0)}t)$$
$$=\exp(+i\omega_c^{(0)}\tau_{\rm seq})\bar{f}_c, \quad (19)$$

where

$$\bar{f}_c=(2\pi)^{-1}\int_0^{2\pi} d\psi\ f_c(\psi). \quad (20)$$

The TOSS centerband amplitude is therefore independent of the angle γ. Equation (19) is provided easily using the fact that $f_c(\psi)$ is a continuous, periodic function of ψ.

Similarly, the γ-average TOSS signal at arbitrary time is given by

$$\langle s_c(t)\rangle^{\rm TOSS}=(2\pi)^{-1}\int_0^{2\pi} d\gamma\ s_c^{\rm TOSS}(t;\gamma)$$
$$=\exp[i\omega_c^{(0)}(t+\tau_{\rm seq})]\bar{f}_c. \quad (21)$$

Note that the time average and the γ average are both related to the same quantity $\bar{f}_c$.

The γ-averaged TOSS signal described in Eq. (21) oscillates evenly in time at the isotropic shift frequency $\omega_c^{(0)}$, while all rotational echoes are suppressed. The γ-averaged sideband amplitudes in the TOSS experiment are therefore

$$\langle a_c^{(k)}\rangle^{\rm TOSS}=\delta_{k0}\,\bar{f}_c\exp(i\omega_c^{(0)}\tau_{\rm seq}). \quad (22)$$

This simple expression indicates the following properties of the carousel-averaged signal.

(i) For a TOSS experiment, in which the magnetization components γ are prepared at the beginning of signal acquisition with phases obeying Eq. (16), the amplitudes of all sidebands $k\neq 0$ are zero.

(ii) The phase and amplitude of the center band depend on the function $\bar{f}_c$, which is in general complex, indicating a phase shift of the signal, characteristic for each carousel.

(iii) There is an additional phase shift proportional to the time-average frequency $\omega_c^{(0)}$, depending on the value $\tau_{\rm seq}$ for the preparation pulse sequence.

The above is a more formal derivation of the rather qualitative arguments originally advanced by Dixon.[2] Subsequent discussions of TOSS employed a rather different treatment based on numerical simulations of magnetization vector trajectories.[5,6] Numerical calculations of the sideband amplitudes $a_c^{(k)}(\gamma)$ for the case of a symmetric chemical shielding tensor ($\eta=0$) led to the conclusion that the suppression of sidebands was caused by "alignment of time-averaged magnetization vectors with the $\pm x$ axis."

In the present nomenclature, "alignment of magnetization vectors with the $\pm x$ axis" implies that the center band amplitudes $a_c^{(0)}(\gamma)^{\rm TOSS}$ are real. However, this is not generally true. The factor $\bar{f}_c$ in Eq. (19) is complex in general. There are no fundamental restrictions on the phase of the center bands in a TOSS experiment.

A more accurate statement is that the center bands of a single carousel are aligned *with each other*. This follows from Eq. (19). The complex amplitudes of the center bands in a TOSS experiment are independent of γ, and all have the same amplitude and phase. The sidebands, on the other hand, have the same amplitude but different phases, and cancel out completely, when a γ average is taken.

This analysis is supported by the numerical simulations shown in Figs. 1 and 2. The complex sideband amplitudes $a_c^{(k)}(\gamma)$ are calculated using

$$a_c^{(k)}(\gamma)=\tau_r^{-1}\int_0^{\tau_r} dt\, s_c(t;\gamma)\exp[-i(\omega_c^{(0)}+k\omega_r)t] \quad (23)$$

for equivalent sites in a number of different orientations. In all cases, the shielding parameters were $\omega_0\Delta\sigma_c/2\pi=3$ kHz, asymmetry parameter $\eta_c=0.5$, and isotropic shift $\omega_c^{\rm iso}=0$. This corresponds to principal elements of the shielding tensor, in frequency units, of 3000, -750, and -2250 Hz. The rotation is at $\omega_r/2\pi=1$ kHz around the magic angle $\tan^{-1}\sqrt{2}$ with respect to the main field. In both figures, a, b, and c are simulations with uniform preparation phase $\phi_c(0;\gamma)=0$; d, e, and f are simulations for a TOSS pulse sequence in which $\phi_c(0;\gamma)$ obeys Eq. (16). In both figures, a and d show the centerband amplitudes $k=0$, b and e show the amplitude of the first sideband on the high-frequency side $k=1$, and c and f show the amplitudes of the second sideband on the high-frequency side $k=2$ for the individual crystallites. In each diagram, the value of $a_c^{(k)}$ for each of the crystallites is shown by a black dot in the complex plane, which is represented by a circle of unit

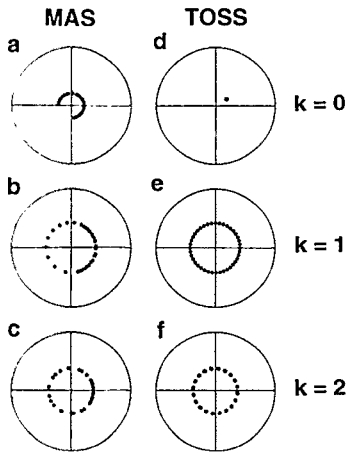

FIG. 1. Complex sideband amplitudes for a single carousel of crystallites in an unmanipulated MAS experiment (a)–(c) and one with TOSS preparation (d)–(f). (a) and (d) show centerband amplitudes ($k=0$); (b) and (e) show amplitudes for the first sideband on the high frequency side ($k=1$); (c) and (f) show amplitudes for the second sideband ($k=2$). The dots show contributions from crystallites with a selection of γ_{PR} values, α_{PR} and β_{PR} being held fixed. Simulation parameters are given in the text.

radius. The real axis (corresponding to positive absorption) is to the right, and the imaginary axis corresponding to dispersion is vertical. At infinite spinning speeds, all dots in the sideband diagrams ($k=1$ and 2) would lie at the origin, and all dots in the center band diagrams ($k=0$) would lie on the unit circle along the positive real axis. At finite spinning speeds, the center band amplitudes are reduced and the sideband amplitudes are increased, and there is a dispersion of amplitudes and phases for the different crystallite orientations, shown visually by the scatter of points over the complex plane.

Figure 1 shows simulations for 40 crystallites with the same angles $\alpha_{PR}=\pi/6$, $\beta_{PR}=\pi/3$, but different values of γ_{PR}. This set of crystallites all lies on the same carousel, with the angle γ_{PR} playing the role of γ in the previous discussion. Without the TOSS preparation, the phase distribution of the sideband components is uneven [Figs. 1(a)–1(c)], although there is a tendency for the sideband amplitudes to be towards the positive real axis, as expected. When TOSS is used [Figs. 1(d)–1(f)], the center bands all have the same phase, as indicated by the superposition of all 40 dots in Fig. 1(d). The sideband phases are now evenly distributed in the complex plane and cancel totally when the average is taken. Note that the dot in Fig. 1(d) does not lie on the real axis—TOSS leads in general to a phase shift of the center bands.

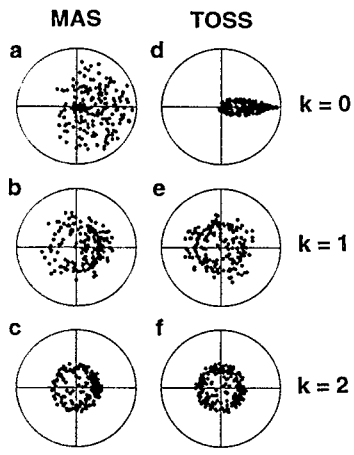

FIG. 2. The same as for Fig. 1, but with a random selection of all three crystallite angles α_{PR}, β_{PR}, and γ_{PR}. (d) shows clearly the distribution of center band phases associated with the TOSS preparation.

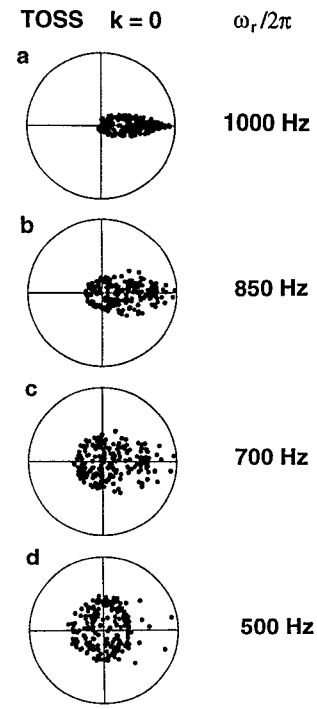

FIG. 3. The effect on the center band amplitudes of reducing the spinning speed. The phase dispersion of center bands becomes worse, leading to a great reduction in the powder-average center band signal.

Figure 2 shows equivalent simulations for a set of 200 crystallites with random values of all three angles $\{\alpha_{PR},\beta_{PR},\gamma_{PR}\}$. The crystallites do not lie on the same carousel in this case. This figure shows clearly the tendency of the center band and sideband amplitudes to cluster along the positive real axis in the ordinary magic-angle-spinning experiment [Figs. 2(a)–2(c)]. For TOSS, the centerband amplitudes are clearly not aligned with each other [Fig. 2(d)]. The phases of the TOSS sidebands are evenly distributed [Figs. 2(e) and 2(f)], leading to vanishing sideband intensities after powder averaging. Note that the average of TOSS centerband amplitudes over an entire powder is real, so no phase shifts are observed in most experimental situations. It is easily shown from Eqs. (1) and (18) that the values of $\bar{f}_c$ for carousels defined by the angles $\{\alpha_{PR},\beta_{PR}\}$ and $\{-\alpha_{PR},\beta_{PR}\}$ are complex conjugates of each other.

Figure 3 shows the result of decreasing the spinning speed in a TOSS experiment on the centerband amplitudes. The partial alignment of Fig. 3(a) rapidly dissolves at

lower spinning speeds. This causes a large reduction of the powder-average center band intensity through destructive interference of the many crystallite components, in agreement with experimental results.[6]

Griffin and co-workers[4–6] may have reached the conclusion that the alignment of magnetization vectors along the $\pm x$ axis was responsible for sideband suppression because their simulations were only performed for the special case of a symmetric shift tensor $\eta=0$. In this case, the frequency Fourier components $\omega_c^{(m)}(\gamma)$ may be chosen to be real for $\gamma=0$. It follows that the factor $\bar{f}_c$ and the TOSS center band amplitude $a_c^{(0)}(\gamma)^{\mathrm{TOSS}}$ are also real if $\omega^{\mathrm{iso}}=0$. The magnetization vectors and center bands are indeed aligned along the $\pm x$ axis in this case. However, *this incidental symmetry is irrelevant to the suppression of the sidebands.*

There is another, deeper problem with the analyses in Refs. 4–6. In these papers, it is shown that for TOSS preparation, in the case $\omega_c^{(0)}=0$, the *time-average phase* of the magnetization vectors is equal to zero. This was then identified as the cause of both the alignment of the magnetization vectors along the $\pm x$ axis and sideband suppression in the simulations. To quote "Alignment causes the time-averaged phase of each magnetization vector to be zero, forcing the center band of each crystallite to be in phase."[6] This sounds plausible, but is incorrect. There is no mathematical relationship between the time-average phase and the center band amplitude (which is the time average of the complex exponential of the phase). To be quite clear, the following three properties are unrelated to each other: (i) the zero value for the time-average phase; (ii) the alignment of centerbands along the $\pm x$ axis for special-case simulations; (iii) sideband suppression. Sideband suppression is a result of carousel symmetries raised in the previous discussion and is *unrelated* to (i) and (ii) above.

These different interpretations could in principle be checked experimentally by performing TOSS experiments on samples with uniaxial order along the rotation axis. The current theory predicts that in general TOSS induces a phase shift of the center band signals, even when the isotropic shift is zero.

Sequences preparing initial magnetization phases satisfying Eq. (16) align the center bands with each other within each carousel, but give in general a dispersion of phases of center bands for different carousels. The question arises as to whether an excitation scheme can be constructed which align center bands not only within each carousel, but also between different carousels. Such a scheme would avoid the intensity losses through destructive interference of out-of-phase signals. In fact, such a state is actually achieved when transverse magnetization is generated by a long weak pulse at the center band frequency, applied to longitudinal magnetization.[17] The center band is enhanced with respect to a normal spectrum and the sidebands are suppressed. However, the selective center band excitation requires prior knowledge of the center band frequency and cannot be used as a technique for spectral simplification. It is an interesting question as to whether a general method can be constructed on these lines.

B. Specific sideband suppression pulse sequences

In the above discussion, we assumed the initial condition (16) without saying how this is actually achieved. In common with previous workers,[2–8] we now discuss specific pulse sequences involving a precession period of length T interrupted by n π pulses at specified times. However, we address the case of n odd as well as n even, and treat explicitly the parameter τ_{seq} describing the phase shifts generated by the isotropic chemical shift.

Assume all transverse magnetization components are prepared with phase 0 at time $t=-T$ (i.e., an interval T before the start of signal acquisition), e.g., by cross polarization or by a strong $\pi/2$ pulse. Strong π pulses are placed at times τ_1, τ_2,...,τ_n after the beginning of the pulse sequence, i.e., at time points $-T+\tau_1$, $-T+\tau_2$,...,$-T+\tau_n$. Assuming strong, perfect π pulses, the magnetization phase at time $t=0$ is given by

$$\phi_c(0)=\Phi_c(0,-T+\tau_n)-\Phi_c(-T+\tau_n,-T+\tau_{n-1})\cdots +(-1)^n\Phi_c(-T+\tau_1,-T) \tag{24}$$

omitting the angle γ for simplicity.

Using Eqs. (8) and (9), this can be written as

$$\phi_c(0)=\omega_c^{(0)}\tau_{\mathrm{seq}}+\xi(0) -(-1)^h\left[2\sum_{q=1}^{n}(-1)^q\xi(-T+\tau_q)+\xi(-T)\right] \tag{25}$$

with

$$\tau_{\mathrm{seq}}=T-2\sum_{q=1}^{n}(-)^{n+q}\tau_q. \tag{26}$$

Equation (16) can therefore be satisfied if the bracketed term in Eq. (25) can be made to vanish. This can in turn be ensured by finding pulse timings for which

$$2\sum_{q=1}^{n}(-1)^q e^{im\theta_q}+1=0 \tag{27}$$

for both $m=1$ and $m=2$, where $\theta_q=\omega_r\tau_q$.

The real and imaginary parts of Eq. (27), for $m=1$ and $m=2$, comprise the four nonlinear TOSS equations.[6] Note that the same equations apply for n even and n odd—only the case of n even has been explored previously.

In practice, it is also desirable that the pulse sequence does not induce any additional phase shifts due to the isotropic shift. This can be ensured by setting $\tau_{\mathrm{seq}}=0$ in Eq. (26). In terms of the angles θ_q, this subsidiary condition can be written

$$-2\sum_{q=1}^{n}(-1)^{n+q}\theta_q+\theta_T=0, \tag{28}$$

where $\theta_T=\omega_r T$. If Eq. (28) can be satisfied for a physically realizable set of angles $0\leqslant\theta_1\leqslant\theta_2\leqslant\cdots\theta_n\leqslant\theta_T$, then the powder-averaged center bands all have the same phase in

the spectrum, within an integer multiple of π. Equation (28) is known as the Hahn echo condition.[2]

C. Analytical solutions for four π pulses

Some numerical solutions for the case $n=4$ have been found.[2,6,8] In Appendix A, we sketch the derivation of the complete set of analytical solutions. There are two branches, with the following values for the timings θ_1, θ_2, θ_3, and θ_4: branch I,

$$\begin{aligned}
\theta_1&=\pi(k-2m)-(-1)^p\,\mathrm{Arccos}[(-1)^k 3/8],\\
\theta_2&=\pi(l-2n)-(-1)^q\,\mathrm{Arccos}[(-1)^l 1/8],\\
\theta_3&=\pi(k+2m)+(-1)^p\,\mathrm{Arccos}[(-1)^k 3/8],\\
\theta_4&=\pi(l+2n)+(-1)^q\,\mathrm{Arccos}[(-1)^l 1/8],
\end{aligned} \tag{29}$$

where p, q, k, l, m, and n are arbitrary integers; branch II,

$$\begin{aligned}
\theta_1&=2\pi k+(-1)^p\,\mathrm{Arccos}\{[-13+(-1)^r 5\sqrt{595}]/152\},\\
\theta_2&=2\pi l+(-1)^p\,\mathrm{Arccos}\{[-51+(-1)^s 7\sqrt{195}]/152\},\\
\theta_3&=2\pi m+(-1)^p\,\mathrm{Arccos}\{[-13-(-1)^r 5\sqrt{595}]/152\},\\
\theta_4&=2\pi n+(-1)^p\,\mathrm{Arccos}\{[-51-(-1)^s 7\sqrt{195}]/152\},
\end{aligned} \tag{30}$$

where p, r, s, k, l, m, and n are arbitrary integers. The timings θ_T of the "Hahn echo" can in each case be found from Eq. (28).

Equations (29) and (30) give the complete set of all possible solutions of TOSS-4. Physically realizable solutions also satisfy $\theta_1<\theta_2<\theta_3<\theta_4$. Some interesting new solutions are presented together with the previously reported sequences in Figs. 4(a)–4(i). The branch number, plus the appropriate values of $p,\ldots,n$ are shown in the figure. The position of the Hahn echo (θ_T) is indicated in most cases by a black circle. If signal acquisition is initiated at this point, the spectrum has no additional frequency-dependent phase shifts.

The shortest possible TOSS-4 sequence is shown in Fig. 4(c). In this case, the Hahn echo is physically inaccessible since $\theta_T<\theta_4$. The position of θ_T is indicated by a white circle. Signal acquisition after the fourth pulse gives a spectrum with strong frequency-dependent phase shifts. However, these may be corrected in the final spectrum, without any detrimental effects, as demonstrated below.

Some more new TOSS-4 sequences are also shown in Figs. 4(e) and 4(g). The pulses are rather evenly spaced compared to previously reported sequences.[2,3,6,8] It will therefore be possible to implement these sequences at very high spinning speeds, unlike known sequences, in which the closely spaced pulses soon start to overlap. However, we should emphasize that the mere absence of overlap does not necessarily imply that a pulse sequence will really function at spinning speeds comparable to the rf field strength.

D. Solutions for five π pulses

The analytical solution for symmetrical TOSS-5 has been already reported.[9] This solution is easily obtained if

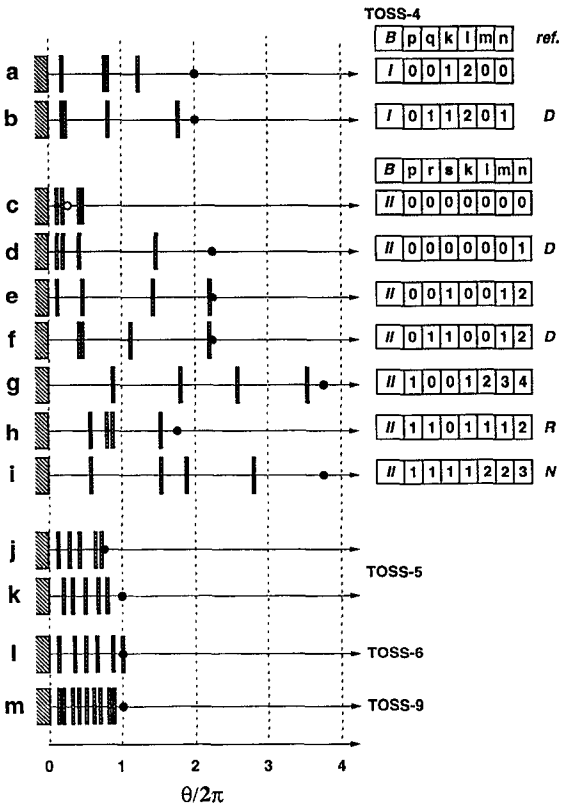

FIG. 4. (a)–(i) A selection of TOSS-4 sequences together with the code specifications from Eqs. (29) and (30) {*B* denotes "branch" of solutions, ref. is references [*D*—Dixon (Ref. 2), *R*—Raleigh *et al.* (Ref. 6), *N*—Nielsen *et al.* (Ref. 8), and sequences without references are new]}. Rectangles show the timings of π pulses in fractions of a rotor period, and black circles show the positions of the "Hahn echo." Sequence (c) has an inaccessible Hahn echo condition before the last π pulse (white circle). Two TOSS-5 sequences (j) and (k) are also shown, and the symmetrical TOSS-6 (l) and TOSS-9 sequences (m).

symmetry is assumed, i.e., $\theta_3=\pi$, $\theta_4=2\pi-\theta_2$, and $\theta_5=2\pi-\theta_1$. The imaginary parts of Eqs. (27) vanish, and we get

$$\begin{aligned}
&-4\cos\theta_1+4\cos\theta_2+3=0 \quad (\text{for } m=1),\\
&-4\cos(2\theta_1)+4\cos(2\theta_2)-1=0 \quad (\text{for } m=2).
\end{aligned} \tag{31}$$

These lead immediately to the solution

$$\begin{aligned}
&\theta_1=\mathrm{Arccos}(7/24), \quad \theta_2=\mathrm{Arccos}(-11/24),\\
&\theta_3=\pi, \quad \theta_4=2\pi-\theta_2, \quad \theta_5=2\pi-\theta_1
\end{aligned} \tag{32}$$

describing a set of symmetrically disposed and almost evenly spaced π pulses contained within a single rotational period [see Fig. 4(k)]. By symmetry, the Hahn echo condition (28) is satisfied for $\theta_T=2\pi$. Signal acquisition should therefore start one whole rotational period after the preparation of the transverse magnetization.

As shown in Ref. 9, it is possible to generate a continuous set of numerical solutions for $n=5$ starting with this analytical solution. One of the five pulses may be shifted slightly in time and the four nonlinear equations solved numerically for the four other pulses. The process can be repeated indefinitely, generating a continuous deformation

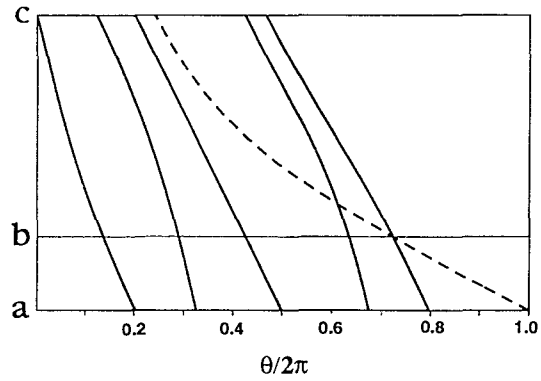

FIG. 5. A continuous set of five π pulse TOSS sequences (solid lines give the π pulse timings) with the Hahn echo condition (broken line). The horizontal axis is time in fractions of a rotational period $2\pi/\omega_r$. Horizontal sections give (a) the symmetrical sequence of 5 π pulses; (b) the shortest known TOSS sequence without a frequency-dependent phase shift (the Hahn echo coincides with the last pulse); (c) the shortest possible TOSS sequence of four π pulses. The first pulse is at zero time and may be omitted; the Hahn echo is inaccessible.

of the initially symmetric five pulse solution [Fig. 5(a)]. An interesting solution found this way corresponds to the values

$$\theta_1/2\pi=0.1366, \quad \theta_2/2\pi=0.2892, \quad \theta_3/2\pi=0.4254, \quad \theta_4/2\pi=0.6341, \quad \theta_5/2\pi=\theta_T/2\pi=0.7227. \tag{33}$$

It is shown in Figs. 4(j) and 5(b). It is the shortest known sequence with a physically accessible Hahn echo. As shown in Ref. 9, further deformation connects this solution to the shortest possible sequence of four π pulses shown in Figs. 4(c) and 5(c).

E. Analytical solution for six π pulses

Figure 5 gives a general key as how to build TOSS-5 from any four π sequence of the complete set of TOSS-4 analytical solutions. Starting with the shortest possible sequence of four π pulses [Fig. 5(c)], the fifth π pulse can be placed at the time origin and shifted slightly in time, while the four nonlinear TOSS equations are solved numerically for the four other pulses. The process can be repeated indefinitely, generating continuous lines of solutions for TOSS-5. A continuous set of numerical solutions for $n=6$ can be generated in analogous fashion starting with any five pulse solution, placing the sixth π pulse at time origin and shifting both it and some other π pulse in time, while the four nonlinear TOSS equations are solved numerically for the four other pulses. This generates six two-dimensional surfaces for timings of six π pulses. The Hahn echo condition is an additional two-dimensional surface.

A pertinent question is whether or not this two-dimensional space of solutions for TOSS-6 contains the shortest possible six π pulse sequence with a physically accessible Hahn echo which is even shorter than the TOSS-5 sequence mentioned above [Fig. 4(j)]. In order to answer this question, we considered only solutions generated from the shortest TOSS-5 [Fig. 4(j)] with the additional constraint that the Hahn echo condition coincides with the last π pulse of TOSS-6 sequences. It was discovered that all such TOSS-6 sequences are in fact longer than the shortest five π pulse TOSS sequence with a physically accessible Hahn echo. One of the interesting TOSS-6 sequences from this set is symmetrical and can also be easily obtained analytically if symmetry is assumed, i.e., $\theta_3=\pi$, $\theta_4=2\pi-\theta_2$, $\theta_5=2\pi-\theta_1$, and $\theta_6=2\pi$. The imaginary parts of Eqs. (27) vanish and we get

$$-4\cos\theta_1+4\cos\theta_2+5=0 \quad (\text{for } m=1), \qquad -4\cos(2\theta_1)+4\cos(2\theta_2)+1=0 \quad (\text{for } m=2). \tag{34}$$

These lead immediately to the solution

$$\theta_1=\text{Arccos}(27/40), \quad \theta_2=\text{Arccos}(-23/40), \quad \theta_3=\pi, \quad \theta_4=2\pi-\theta_2, \quad \theta_5=2\pi-\theta_1, \quad \theta_6/2\pi=\theta_T/2\pi=2\pi \tag{35}$$

describing a set of symmetrically disposed and almost evenly spaced π pulses contained within a single rotational period [see Fig. 4(l)]. By symmetry, the Hahn echo condition (28) is satisfied for $\theta_T=2\pi$.

F. Analytical solution for nine π pulses

Dixon[18] reported two eight-pulse TOSS sequences which satisfy Eqs. (27) for $m=3$ and 4 as well as for $m=1$ and 2. It was proposed without demonstration that these sequences could be useful for spinning sideband suppression in magic-angle-spinning spectroscopy of half-integer spin nuclei with second-order quadrupolar interactions. These sequences are very difficult to demonstrate, not least because quadrupolar nuclei often have short T_2 values and Dixon's eight π pulse sequences are rather long. We point out here an additional solution consisting of a symmetrical set of nine π pulses occupying only a single rotor period [Fig. 4(m)]. The analytical solution is given in Appendix B.

It is doubtful, however, that these sequences will be of much use for applications to quadrupolar nuclei, mainly because it will be very difficult to control pulse imperfections after eight or nine pulses. It is also hard to identify a good motivation for sideband suppression in this case anyway. The sequence may find a use in spinning sideband suppression of liquid samples rotating in a very inhomogeneous magnetic field.

III. EXPERIMENT

All NMR experiments were performed at a magnetic field of 4.7 T using a Bruker MSL 200 spectrometer. An external ENI LPI-10H amplifier with high stability and pulse-shape performance was employed in the ^{13}C or ^{31}P channels of the spectrometer ($\omega_1/2\pi=109$ kHz). An additional circuit for gating of this external device was built. A standard Bruker double bearing 4 mm rotor system (ZrO_2 rotors, Kel-F end caps) was used. *L*-tyrosine hy-

drochloride powder (Sigma) was used without further purification. Diammonium orthophosphite $(NH_4)_2HPO_3$ (DAOP) was obtained by dissolving ammonium hydroxide (Sigma) to saturation in phosphorous acid (Sigma) with subsequent removal of water. The ^{13}C or ^{31}P magic-angle-spinning spectra were obtained using cross polarization from the protons[19] with mixing time 5 ms. The proton rf field was enhanced by 3 dB during the TOSS sequence to avoid Hartmann–Hahn matching during the ^{13}C or ^{31}P pulses. In most cases, the effects of pulse imperfections were reduced by independent phase cycling[20] of each π pulse in steps of $2\pi/3$, and adjustment of the receiver reference phase, to select the appropriate coherence transfer pathways

$$(+1)\rightarrow(-1)\rightarrow(+1)\rightarrow(-1)\rightarrow(+1)\rightarrow(-1)$$

(for five π pulses) and

$$(-1)\rightarrow(+1)\rightarrow(-1)\rightarrow(+1)\rightarrow(-1)$$

(for four π pulses).

IV. EXPERIMENTAL RESULTS

Figure 6 represents ^{13}C magic-angle-spinning ($\omega_r/2\pi = 2.000$ kHz) spectra of *L*-tyrosine hydrochloride powder using cross polarization from the protons.[19] Figure 6(a) shows the ordinary CP/MAS spectrum revealing numerous overlapping sidebands. With the shortest TOSS sequence of four π pulses presented in Fig. 4(c) the sidebands are effectively suppressed [Fig. 6(b)] and many of the center bands are enhanced, as described previously.[4,6] This sequence generates strong frequency-dependent phase shifts since the Hahn echo condition (28) cannot be satisfied. Nevertheless, the phase can be successfully corrected after Fourier transformation apparently without significant distortion of the spectrum. This sequence occupies only 0.4670 of a rotor period and is even shorter than the newly reported SELTICS (which gives rise to large phase shifts as well[14]).

An almost identical spectrum [Fig. 6(c)] is obtained using the shortest known TOSS sequence of five π pulses [Fig. 4(j)]. This pulse sequence has no frequency-dependent phase shifts and occupies less than one rotor period (0.7227). It is an alternative to the symmetrical sequence of five π pulses presented previously.[9] These two short TOSS sequences are of particular interest for systems with short transverse relaxation times.

Figure 7 shows ^{31}P results on diammonium orthophosphite (DAOP) powder, spinning at 2630 Hz. The normal MAS spectrum is shown in Fig. 7(a). A spectrum using the symmetrical TOSS-5 sequence is shown in Fig. 7(b). For this spectrum, phase cycling was not used. Clearly, acceptable sideband suppression is achieved without this precaution, providing care is taken to achieve well-adjusted π pulses. To produce this spectrum, the five π pulses had constant phases of 0°, 330°, 60°, 330°, and 0°, respectively. We found empirically that this sequence of phases, used by Tycko *et al.*[21] in the context of composite inversion pulses, gave somewhat better sideband suppression than when all pulses had the same phase. The cause is unknown. In Fig. 7(c), we achieved very good sideband suppression by employing a long phase cycle with the phase of all 5 π pulses varied in steps of $2\pi/3$.

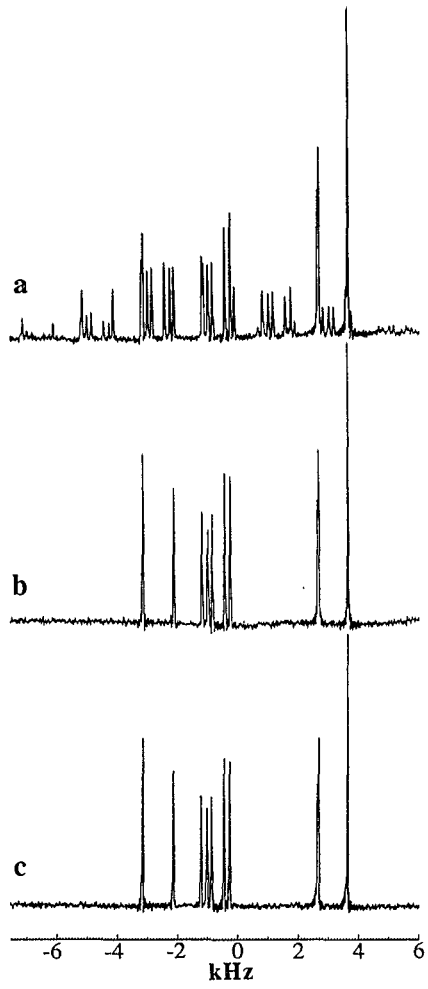

FIG. 6. ^{13}C spectra of *L*-tyrosine hydrochloride powder (the sum of 486 transients). (a) Normal CP/MAS; (b) the shortest TOSS with four π pulses [Fig. 4(c)] after the correction for frequency-dependent phase shifts; (c) the shortest TOSS sequence of five π pulses [Fig. 4(j)].

V. CONCLUSIONS

It is possible to understand sideband suppression in rotating powdered solids by rather general symmetry arguments based on the identification of carousels of molecular sites, related to each other by a rotation around the spinning axis. This analysis predicts center band phase shifts induced by the anisotropic interactions, in disagreement with previous theoretical approaches. For a totally disordered powder sample, however, these phase shifts are not visible because of additional interference between different carousel signals. Nevertheless, it may be important to take the phase shifts into account in experiments on samples which are not totally disordered.

The complete set of analytical solutions of the TOSS equations for four π pulses has been found. The analytical set of solutions includes those previously reported and

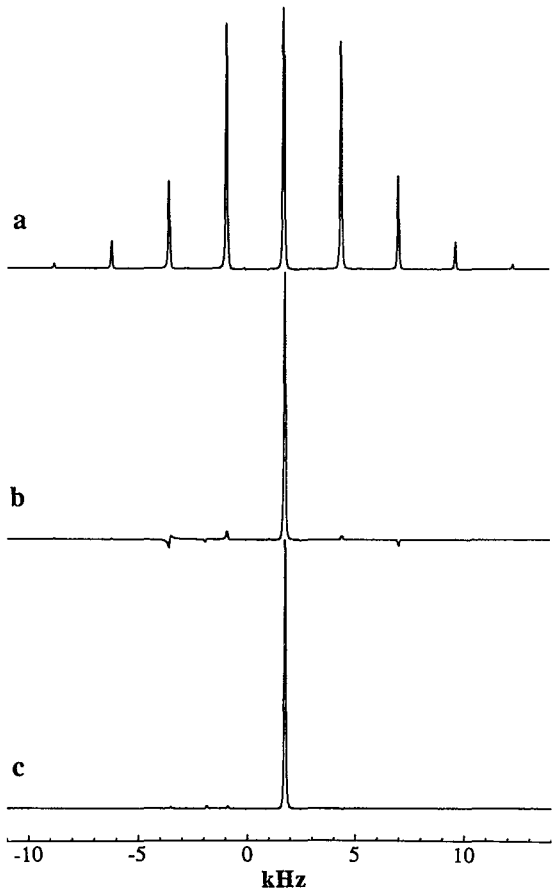

FIG. 7. ^{31}P spectra of diammonium orthophosphite powder (the sum of 243 transients). (a) Normal CP/MAS; (b) symmetrical five pulse TOSS [Fig. 4(k)] with constant π pulse phases 0, 330, 60, 330, 0; (c) symmetrical five pulse TOSS with a long phase cycle to suppress pulse imperfections.

some interesting new possibilities. The shortest TOSS-4 sequence occupies only 0.4670 of a rotor period, but generates strong frequency-dependent phase shifts. It was shown experimentally that the phase shifts can be corrected after Fourier transformation without significant distortion.

A continuous set of TOSS-5 sequences has also been derived. The shortest TOSS-5 sequence with an accessible Hahn echo covers only ~ 0.72 of a single rotational period and has been demonstrated experimentally.

It should be emphasized that all these sequences, as well as the SELTICS sequences,[14] prepare an essentially indistinguishable initial condition for the magnetization components. At low spinning speed, all sequences suffer from a destruction of the center band intensities due to the spread in phases of the different crystallite contributions. This loss in intensity may in principle be recovered by two-dimensional experiments.[12]

We have not ventured to compare the TOSS sequences of π pulses with the SELTICS method,[14] which uses phase-alternated continuous rf bursts. One of the reported advantages of SELTICS is that the pulse sequences are much shorter than TOSS. This now seems to be an overstatement and, in fact, TOSS sequences can be designed which are even shorter than SELTICS. The other reported advantage of SELTICS is that it is less sensitive to pulse imperfections. This charge has more merit, but in practice, the relative performance may depend on the spectrometer. TOSS may be more sensitive to radiofrequency inhomogeneity, while SELTICS may be more sensitive to radiofrequency droop.

ACKNOWLEDGMENTS

This work has been supported by the Swedish Natural Science Research Council. The MSL 200 spectrometer was purchased with a grant from the Knut and Alice Wallenberg Foundation. We would like to thank N. C. Nielsen and S. C. Shekar for discussions and G. S. Harbison for suggesting a suitable sample and supplying a preprint of Ref. 14.

APPENDIX A: ANALYTICAL SOLUTIONS FOR FOUR π PULSE TOSS

We start from the TOSS equations

$$2\sum_{q=1}^{4}(-1)^q e^{im\theta_q}+1=0, \quad m=1,2. \tag{A1}$$

The real and imaginary parts of Eq. (A1) comprise four separate equations. They may be transformed into the system

$$\sin(\alpha/2)\cos(\beta/2)=\sin(\gamma/2)\cos(\delta/2), \tag{A2a}$$

$$\sin\alpha\cos\beta=\sin\gamma\cos\delta \tag{A2b}$$

$$-\cos(\alpha/2)\cos(\beta/2)+\cos(\gamma/2)\cos(\delta/2)+1/4=0, \tag{A2c}$$

$$-\cos\alpha\cos\beta+\cos\gamma\cos\delta+1/4=0, \tag{A2d}$$

where

$$\alpha=\theta_1+\theta_3, \quad \beta=\theta_3-\theta_1, \quad \gamma=\theta_2+\theta_4, \quad \delta=\theta_4-\theta_2. \tag{A3}$$

We can identify two different branches of solutions.

1. Branch I

Equations (A2a) and (A2b) are satisfied trivially if

$$\sin(\alpha/2)=\sin(\gamma/2)=0. \tag{A4}$$

The general solution of Eq. (A4) is $\alpha=2\pi k$, $\gamma=2\pi l$, where k, $l=0, \pm 1, \pm 2,\ldots$. Equations (A2c) and (A2d) may then be written

$$-(-1)^k\cos(\beta/2)+(-1)^l\cos(\delta/2)=-1/4, \tag{A5a}$$

$$-\cos\beta+\cos\delta=-1/4. \tag{A5b}$$

Equation (A5b) can be rewritten in terms of $\beta/2$ and $\delta/2$ as

$$[\cos(\beta/2)-\cos(\delta/2)][\cos(\beta/2)+\cos(\delta/2)]=1/8. \tag{A6}$$

Substituting Eq. (A5a) in Eq. (A6) for different k and l, we can rewrite the system of Eqs. (A5) in the form

$$\cos(\beta/2)-(-1)^{k+l}\cos(\delta/2)=(-1)^k/4,$$
$$\cos(\beta/2)+(-1)^{k+l}\cos(\delta/2)=(-1)^k/2. \tag{A7}$$

Solutions of Eqs. (A7) can be easily found

$$\beta=(-1)^p\,2\,\mathrm{Arccos}\{(-1)^k 3/8\}+4\pi m,$$
$$\delta=(-1)^q 2\,\mathrm{Arccos}\{(-1)^l 1/8\}+4\pi n, \tag{A8}$$

where p, q, m, and n are arbitrary integers.

Finally, using the solutions of Eq. (A4) and the conditions of Eq. (A3), we can derive the *branch I* solutions

$$\theta_1=\pi(k-2m)-(-1)^p\,\mathrm{Arccos}[(-1)^k 3/8],$$
$$\theta_2=\pi(l-2n)-(-1)^q\,\mathrm{Arccos}[(-1)^l 1/8],$$
$$\theta_3=\pi(k+2m)+(-1)^p\,\mathrm{Arccos}[(-1)^k 3/8], \tag{A9}$$
$$\theta_4=\pi(l+2n)+(-1)^q\,\mathrm{Arccos}[(-1)^l 1/8],$$

where p, q, k, l, m, and n are arbitrary integers.

The Hahn echo condition (28) is given by the simple formula

$$\theta_T=4\pi(l-k). \tag{A10}$$

Physically realizable solutions can be found from Eq. (A9) using the property $\theta_1<\theta_2<\theta_3<\theta_4$.

2. Branch II

Starting from the system (A2), $\cos(\beta/2)$ and $\cos(\delta/2)$ may be derived as functions of α and γ from Eqs. (A2a) and (A2b)

$$\cos(\beta/2)=\pm\sqrt{\{\sin^2(\alpha/2)[\sin\alpha-\sin\gamma]/[\sin\alpha-\sin\gamma+\sin(\gamma-\alpha)]\}}, \tag{A11a}$$

$$\cos(\delta/2)=\pm\sqrt{\{\sin^2(\gamma/2)[\sin\alpha-\sin\gamma]/[\sin\alpha-\sin\gamma+\sin(\gamma-\alpha)]\}}, \tag{A11b}$$

where $\sin(\alpha/2)\neq 0$, $\sin(\gamma/2)\neq 0$, $\sin\alpha\neq 0$, and $\sin\gamma\neq 0$.

After substitution of $\cos(\beta/2)$ and $\cos(\delta/2)$ into Eqs. (A2c), and (A2d), we get a system of two equations

$$(\sin\alpha-\sin\gamma)[7-8\cos(\gamma\pm\alpha)]=\sin(\gamma-\alpha),$$
$$(\cos\gamma-\cos\alpha)[7-8\cos(\gamma\pm\alpha)]=2[1-\cos(\gamma\pm\alpha)]. \tag{A12}$$

Plus signs in Eqs. (A12) correspond to equal signs in Eqs. (A11). Minus signs in Eqs. (A12) correspond to opposite signs in Eqs. (A11).

We show later that only the set of equations with minus signs in Eqs. (A12) leads to true solutions of the TOSS equations. These may be transformed into the form

$$x(15-16y^2)=-y,$$
$$[\pm\sqrt{(1-x^2)}](15-16y^2)=-2[\pm\sqrt{(1-y^2)}], \tag{A13}$$

where $x=\cos[(\gamma+\alpha)/2]$, $y=\cos[(\gamma-\alpha)/2]$, $-1\leqslant x\leqslant 1$, and $-1\leqslant y\leqslant 1$.

The general solutions of Eqs. (A13) are

$$[x,y]=\{[\pm 1,\pm 1],\quad [\pm(\sqrt{221})/19,\pm(-\sqrt{221})/16]\}. \tag{A14}$$

However, the first two solutions may be rejected since they correspond to $\sin(\alpha/2)=\sin(\gamma/2)=0$, in contradiction to Eqs. (A11). The latter two solutions may readily be transformed back into following two possibilities for the angles α, β, γ, and δ:

$$\cos\alpha=\cos(\theta_1+\theta_3)=-291/304,$$
$$\cos\beta=\cos(\theta_3-\theta_1)=-6/19,$$
$$\cos\gamma=\cos(\theta_2+\theta_4)=-151/304, \tag{A15a}$$
$$\cos\delta=\cos(\theta_4-\theta_2)=-2/19,$$

or

$$\cos\alpha=-151/304,\quad \cos\beta=-2/19,$$
$$\cos\gamma=-291/304,\quad \cos\delta=-6/19. \tag{A15b}$$

The solution of Eqs. (A15b) can be shown to be spurious, generated by loss of sign information when factors are squared. The system of Eqs. (A15a) can readily be solved for the timings θ_q,

$$\begin{cases}\cos\theta_1=[-13\pm 5\sqrt{595}]/152,\\ \cos\theta_3=[-13\pm(-5\sqrt{595})]/152,\end{cases}$$
$$\begin{cases}\cos\theta_2=[-51\pm 7\sqrt{195}]/152,\\ \cos\theta_4=[-51\pm(-7\sqrt{195})]/152,\end{cases} \tag{A16}$$

where upper or bottom signs are kept in pairs only.

After further analysis of signs and rejection of spurious solutions, we get the general result

$$\theta_1=2\pi k+(-1)^p\,\mathrm{Arccos}\{[-13+(-1)^r 5\sqrt{595}]/152\},$$
$$\theta_2=2\pi l+(-1)^p\,\mathrm{Arccos}\{[-51+(-1)^s 7\sqrt{195}]/152\},$$
$$\theta_3=2\pi m+(-1)^p\,\mathrm{Arccos}\{[-13-(-1)^r 5\sqrt{595}]/152\}, \tag{A17}$$
$$\theta_4=2\pi n+(-1)^p\,\mathrm{Arccos}\{[-51-(-1)^s 7\sqrt{195}]/152\},$$

where p, r, s, k, l, m, and n are arbitrary integers. Physically realizable solutions also satisfy $\theta_1<\theta_2<\theta_3<\theta_4$.

To complete the analysis of *branch II*, the system of Eqs. (A12) with plus signs should be discussed as well. All analytical solutions of it were found and analyzed using a method similar to the one presented above. However, it was discovered that all these solutions are in fact spurious and lead to sign disagreements. We conclude that Eqs. (A9) and (A17) are the complete set of all possible solutions of the system of TOSS equations (A1).

APPENDIX B: ANALYTICAL SOLUTIONS FOR SYMMETRICAL NINE π PULSE TOSS

We start from the general form of TOSS equations

$$2\sum_{q=1}^{9}(-1)^q e^{im\theta_q}+1=0, \tag{B1}$$

where $m=1$, 2, 3, and 4, and assuming symmetry $\theta_5=\pi$, $\theta_6=2\pi-\theta_4$, $\theta_7=2\pi-\theta_3$, $\theta_8=2\pi-\theta_2$, and $\theta_9=2\pi-\theta_1$.

The imaginary parts of Eqs. (B1) vanish and we get

$$-4\cos m\theta_1+4\cos m\theta_2-4\cos m\theta_3+4\cos m\theta_4 +2(-1)^{m+1}+1=0. \tag{B2}$$

The system of Eqs. (B2) can be transformed to

$$\begin{aligned} &-\cos\theta_1+\cos\theta_2-\cos\theta_3+\cos\theta_4=-3/4,\\ &-\cos^2\theta_1+\cos^2\theta_2-\cos^2\theta_3+\cos^2\theta_4=1/8,\\ &-\cos^3\theta_1+\cos^3\theta_2-\cos^3\theta_3+\cos^3\theta_4=-3/4,\\ &-\cos^4\theta_1+\cos^4\theta_2-\cos^4\theta_3+\cos^4\theta_4=5/32. \end{aligned} \tag{B3}$$

A physically meaningful solution to this system of equations was found by computer algebra

$$\begin{aligned} \cos\theta_1&=[407+\sqrt{1\,973\,357}]/2576,\\ \cos\theta_2&=[-4472+24\sqrt{249\,029}]/20\,608,\\ \cos\theta_3&=[3256-8\sqrt{1\,973\,357}]/20\,608,\\ \cos\theta_4&=[-559-3\sqrt{249\,029}]/2576. \end{aligned} \tag{B4}$$

In fractions of a rotor period, the timings are

$$\{\theta_1,\ldots,\theta_9\}/2\pi=\{0.1258,\ 0.1907,\ 0.3133,\ 0.3971,\ 0.5000,\ 0.6029,\ 0.6867,\ 0.8093,\ 0.8742\}.$$

By symmetry, the Hahn echo condition (28) is satisfied for $\theta_T=2\pi$.

[1] M. M. Maricq and J. S. Waugh, J. Chem. Phys. **70**, 3300 (1979).
[2] W. T. Dixon, J. Chem. Phys. **77**, 1800 (1982).
[3] W. T. Dixon, J. Schaeffer, M. D. Sefcik, E. O. Stejskal, and R. A. McKay, J. Magn. Reson. **49**, 341 (1982).
[4] E. T. Olejniczak, S. Vega, and R. G. Griffin, J. Chem. Phys. **81**, 4804 (1984).
[5] D. P. Raleigh, E. T. Olejniczak, S. Vega, and R. G. Griffin, J. Magn. Reson. **72**, 238 (1987).
[6] D. P. Raleigh, E. T. Olejniczak, and R. G. Griffin, J. Chem. Phys. **89**, 1333 (1988).
[7] M. A. Hemminga and P. A. de Jager, J. Magn. Reson. **51**, 339 (1983).
[8] N. C. Nielsen, H. Bildsøe, and H. J. Jakobsen, J. Magn. Reson. **80**, 149 (1988).
[9] Z. Song, O. N. Antzutkin, X. Feng, and M. H. Levitt, Solid State Nucl. Magn. Reson. **2**, 143 (1993).
[10] A. C. Kolbert and R. G. Griffin, Chem. Phys. Lett. **166**, 87 (1990).
[11] H. Geen and G. Bodenhausen, J. Chem. Phys. **97**, 2928 (1992).
[12] H. Geen and G. Bodenhausen, J. Am. Chem. Soc. **115**, 1579 (1993).
[13] A. Hagemeyer, K. Schmidt-Rohr, and H. W. Spiess, Adv. Magn. Reson. **13**, 85 (1989).
[14] J. Hong and G. S. Harbison, J. Magn. Reson. (in press).
[15] M. H. Levitt, J. Magn. Reson. **82**, 427 (1989).
[16] M. Mehring, *High Resolution NMR in Solids* (Springer, Berlin, 1982).
[17] P. Caravatti, G. Bodenhausen, and R. R. Ernst, J. Magn. Reson. **55**, 88 (1983).
[18] W. T. Dixon, J. Magn. Reson. **64**, 332 (1985).
[19] A. Pines, M. G. Gibby, and J. S. Waugh, J. Chem. Phys. **59**, 569 (1973).
[20] G. Bodenhausen, H. Kogler, and R. R. Ernst, J. Magn. Reson. **58**, 370 (1984).
[21] R. Tycko, A. Pines, and J. Guckenheimer, J. Chem. Phys. **83**, 2775 (1985).